# Landau-Forbidden Quantum Criticality in Rydberg Quantum Simulators

Jong Yeon Lee,[1,*] Joshua Ramette,[2,3] Max A. Metlitski,[2] Vladan Vuletić,[2,3] Wen Wei Ho,[4,5,6] and Soonwon Choi[2,7]

[1]*Kavli Institute for Theoretical Physics, University of California, Santa Barbara, California 93106, USA*
[2]*Department of Physics, Massachusetts Institute of Technology, Cambridge, Massachusetts 02139, USA*
[3]*Research Laboratory of Electronics, Massachusetts Institute of Technology, Cambridge, Massachusetts 02139, USA*
[4]*Department of Physics, Stanford University, Stanford, California 94305, USA*
[5]*Department of Physics, National University of Singapore, Singapore 117542*
[6]*Centre for Quantum Technologies, National University of Singapore, 3 Science Drive 2, Singapore 117543*
[7]*Laboratory for Nuclear Science, Massachusetts Institute of Technology, Cambridge, Massachusetts 02139, USA*

(Received 27 July 2022; revised 27 November 2022; accepted 31 July 2023; published 22 August 2023)

The Landau-Ginzburg-Wilson theory of phase transitions precludes a continuous transition between two phases that spontaneously break distinct symmetries. However, quantum mechanical effects can intertwine the symmetries, giving rise to an exotic phenomenon called deconfined quantum criticality (DQC). In this Letter, we study the ground state phase diagram of a one-dimensional array of individually trapped neutral atoms interacting strongly via Rydberg states, and demonstrate through extensive numerical simulations that it hosts a variety of symmetry-breaking phases and their transitions including DQC. We show how an enlarged, emergent continuous symmetry arises at the DQCs, which can be experimentally observed in the joint distribution of two distinct order parameters, obtained within measurement snapshots in the standard computational basis. Our findings highlight quantum simulators of Rydberg atoms not only as promising platforms to experimentally realize such exotic phenomena, but also as unique ones allowing access to physical properties not obtainable in traditional experiments.

DOI: 10.1103/PhysRevLett.131.083601

The modern theory of continuous phase transitions is rooted in the Landau-Ginzburg-Wilson (LGW) framework. The central idea is to describe phases and their transitions using order parameters: local observables measuring spontaneous symmetry breaking (SSB). In recent years, however, new kinds of critical behavior beyond this paradigm have been shown to exist. For example, quantum phase transitions (QPT) between phases with and without topological order are characterized not by symmetry breaking but rather by singular changes in patterns of long-range quantum entanglement. Another example is the continuous QPT between distinct SSB phases of certain two-dimensional magnets [1,2]. Such a scenario is generally forbidden within the LGW framework since there is no *a priori* reason why the order parameter of one phase vanishes *concomitantly* as the order parameter of another develops.

Deconfined quantum criticality (DQC) is a unifying framework proposed to explain such unconventional behavior: instead of order parameters, these critical points are described by emergent fractionalized degrees of freedom interacting via deconfined gauge fields. This can lead to interesting measurable consequences in macroscopic phenomena, such as emergent symmetries and accompanying conserved currents [3–7]. However, despite numerous experimental proposals and attempts [6,8–30], DQC is still a largely theoretical concept, and an unambiguous experimental observation remains to be made.

In this Letter, we propose programmable quantum simulators based on arrays of Rydberg atoms as promising platforms to realize and verify DQC. These are systems of atoms individually trapped by optical tweezers, and pumped by lasers to highly excited Rydberg states through which they interact. Owing to their wide programmability, a host of interesting quantum many-body phenomena can be simulated [31–36]. Here, we similarly leverage their programmability to present a realistic model of interacting spin-$\frac{1}{2}$ particles in 1D, and show that a host of SSB phases and QPTs, including DQC, arise [Figs. 1(a) and 1(b)]. Furthermore, we demonstrate the emergence of an enlarged, continuous symmetry—a smoking gun signature of DQC—is readily observable in experiments through the joint distribution of two order parameters over global measurement snapshots [Figs. 1(c)–1(e)].

*Model.*—We study an array of neutral atoms trapped in optical tweezers and arranged in a 1D zigzag structure [Fig. 1(a)], with periodic boundary conditions imposed by closing the chain into a ring. An effective spin-$\frac{1}{2}$ degree of freedom $\{|\uparrow\rangle, |\downarrow\rangle\}$ is taken to be encoded by distinct highly excited Rydberg states of each atom [Fig. 1(a)]. Then, the combination of dipolar and Van der Waals interactions among Rydberg atoms naturally induces the following effective Hamiltonian for spins:

 

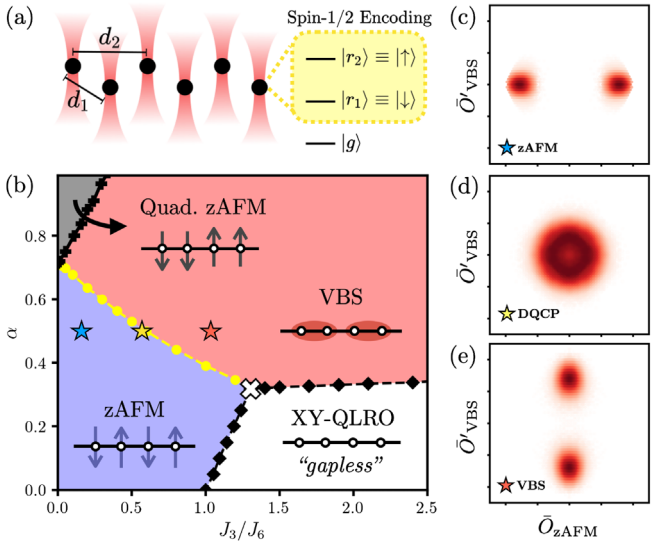


FIG. 1. (a) Zigzag arrangement of atoms and spin-$\frac{1}{2}$ encoding utilizing Rydberg states. (b) Ground state phase diagram of $H_{\rm eff}$. Red, blue, black, and white regions correspond to VBS, zAFM, quadrupled zAFM, and gapless XY phases respectively. Solid points are extracted numerically by the finite-size scaling. Dashed (solid) lines depict (dis)continuous QPTs. Yellow (black) dashed lines are deconfined quantum (BKT) critical points. (c)–(e) Joint distribution of zAFM and VBS order parameters over $2 \times 10^4$ $z$-basis snapshots, computed at the three different markers in the phase diagram ($L = 192$). The ring-shaped distribution in (d) is the hallmark of an emergent U(1) symmetry arising at the DQCP.

$$H_{\rm eff} = J_3 \sum_r [(X_r X_{r+1} + Y_r Y_{r+1}) + \alpha (X_r X_{r+2} + Y_r Y_{r+2})] + J_6 \sum_r [Z_r Z_{r+1} + \alpha^2 Z_r Z_{r+2}] + H_{\rm LR}. \quad (1)$$

Above, $X, Y, Z$ are standard Pauli matrices; $J_3, J_6$ quantify strengths of spin-exchange and Ising interactions for nearest-neighbor pairs of atoms respectively; $\alpha \equiv (d_1/d_2)^3$ and $\alpha^2$ govern the relative strengths of the different nearest-neighbor (NN) to next nearest-neighbor (NNN) couplings, where $d_1(d_2)$ is the NN (NNN) atomic distance. $H_{\rm LR}$ contains long-range terms beyond NNN arising from both dipolar and Van der Waals (VdW) interactions, which decay with distance as $1/r^3$ and $1/r^6$ respectively. $H_{\rm eff}$ is distinct from conventional Hamiltonians previously realized in Rydberg simulators [31–34]: it contains *both* Ising and exchange couplings. Importantly, we assume the ability to independently tune parameters $(\alpha, J_3/J_6)$ over a wide range of values; we will demonstrate how to achieve this experimentally later.

*Quantum phases.*—We aim to ascertain the ground state phase diagram of $H_{\rm eff}$ over $(\alpha, J_3/J_6)$ at zero magnetization. By inspecting its symmetries, translation symmetry with a spin-$\frac{1}{2}$ per unit cell, $\mathrm{U}(1)_z \times \mathbb{Z}_2^x$ symmetry (spin rotation [spin flip] about the $z[x]$ axis respectively), and site-centered inversion symmetry $\mathcal{I}$, one can already declare that all phases must either be SSB or gapless. This stems from the Lieb-Schultz-Mattis theorem [37–40], which forbids a gapped disordered phase under such symmetry considerations.

Salient features of the phase diagram can be understood upon truncating $H_{\rm eff}$ to at most NNN terms, i.e., ignoring $H_{\rm LR}$ [41–43]. When $J_3 = 0$, the system is purely classical [44]. There is however a competition (tuned by $\alpha$) between NN Ising interactions, which induce antiferromagnetic (zAFM) order in the $z$ direction that spontaneously breaks the $\mathbb{Z}_2^x$ spin-flip symmetry, and NNN Ising interactions, which induce instead so-called quadrupled antiferromagnetic order (QzAFM), further breaking $\mathcal{I}$. These phases are separated by a first-order transition at $\alpha = 1/\sqrt{2}$ (modified with $H_{\rm LR}$). When $\alpha = 0$, the model reduces to the familiar $XXZ$ model, which hosts zAFM order at $J_3 < J_6$, and a symmetric but gapless $XY$ phase with quasilong range order (XY QLRO) at $J_3 > J_6$. A final limiting case is when $\alpha = 1/2$ and $J_3/J_6 \to \infty$, called the Majumdar-Ghosh point [45]. There, the valence bond solid (VBS) states describing dimerized patterns of spin singlets are the ground states, which spontaneously break $\mathcal{I}$. Caricatures of the different orders are shown in Fig. 1(b).

We numerically verify the presence of all these phases for the full model $H_{\rm eff}$ with long-range interactions. Concretely, we consider the order parameters

$$O_{\rm zAFM}(r) \equiv e^{i\pi r} Z_r, \qquad O_{\rm QzAFM}(r) \equiv e^{i\pi r/2} Z_r,$$
$$O_{\rm VBS}(r) \equiv e^{i\pi r} [\vec{S}_{r+1} \cdot \vec{S}_r - \vec{S}_r \cdot \vec{S}_{r-1}], \quad (2)$$

which measure violations of symmetries: $\mathbb{Z}_2^x$ with wave vector $\pi$ and $\pi/2$, and $\mathcal{I}$ respectively. We also consider their correlations $C_a(r) \equiv \langle O_a(0) O_a(r) \rangle$, and $C_{XY}(r) \equiv \langle X(0)X(r) \rangle = \langle Y(0)Y(r) \rangle$ detecting ordering in the easy plane. Employing a density-matrix renormalization group (DMRG) algorithm for infinite systems [46–48], we compute Eq. (2) along various cuts of the phase diagram.

Focusing first along a vertical cut $J_3/J_6 = 0.1$ [Fig. 2(a)], we see that for $\alpha < \alpha_{c1} = 0.678(1)$, the system is zAFM ordered, evinced by a nonzero $O_{\rm zAFM}$ and vanishing $O_{\rm VBS}$ [49]. When $\alpha_{c1} < \alpha < \alpha_{c2} = 0.787(1)$, the converse happens, indicating the system is VBS ordered. For $\alpha > \alpha_{c2}$, another phase appears wherein $O_{\rm VBS}$ remains nonzero, while $O_{\rm QzAFM}$ appears in discontinuous fashion; this is the QzAFM phase. The derivative of the ground state energy across this transition is seen not to be smooth, indicating that it is a first-order transition. For the horizontal cut $\alpha = 0.5$, we see the system has zAFM(VBS) order to the left (right) of $J_3/J_6 = 0.5968$ [Fig. 2(b)]. Interestingly, the two order parameters, $O_{\rm zAFM}$ and $O_{\rm VBS}$, appear to vanish-appear continuously precisely at this same point—indication that this QPT is unconventional. Further evidence of its continuous nature is provided by a divergent correlation length seen in DMRG

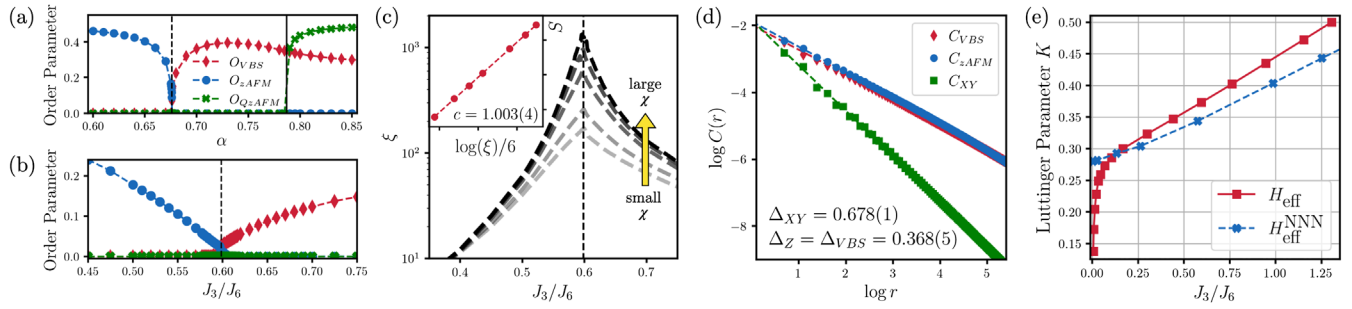


FIG. 2. (a),(b) Magnitudes of spatially averaged VBS, zAFM, and QzAFM order parameters along different cuts in the phase diagram. (a) $J_3/J_6 = 0.1$. The system is zAFM(VBS) ordered to the left(right) of the critical point $\alpha_{c1} \sim 0.677$. Past $\alpha_{c2} \sim 0.787$ the system transitions to QzAFM. (b) $\alpha = 0.5$. The system is zAFM(VBS) ordered to the left(right) of the critical point $J_3/J_6 \sim 0.5968$, whereupon both order parameters vanish with increasing bond dimension in DMRG numerics (and therefore correlation length $\xi$) [51]. (c) Divergence of correlation lengths at the critical point of (b) with increasing bond dimension $\chi = 70, 100, 200, 300, 400$. Inset: scaling of entanglement entropy versus (log) correlation length yields a slope $c = 1$. (d) Correlation functions behavior at the critical point of (b). (e) Luttinger parameter $K$, extracted from exact numerical calculations and finite-size scaling analysis, along the DQCP line in the phase diagram of $H_{\text{eff}}$, and its NNN truncation $H_{\text{eff}}^{\text{NNN}}$.

simulations with increasing accuracy, enabled by increasing bond dimension [Fig. 2(c)]; scaling of the von Neumann entanglement entropy with correlation length also yields a central charge $c = 1$ [50], indicative of an underlying conformal field theory. Lastly, on the horizontal cut $\alpha = 0.2$ (see the Supplemental Material [51]), at small $J_3/J_6$ we observe that $O_{\text{zAFM}}$ is nonzero as expected, while it goes very smoothly to zero for larger $J_3/J_6$, with no obvious discontinuity in any of its derivatives. This suggests that the crossed QPT is of Berezinskii-Kosterlitz-Thouless (BKT) type [52,53]. Similarly, the QPT between $XY$ and VBS along the horizontal cut of the diagram is of BKT, which is proposed to be of DQC point (DQCP) in two-dimensional quantum magnet [1,2]. Plots of the zAFM, VBS, and $XY$ correlation functions in the large $J_3/J_6$ regime yield that they all decay with power laws, with $C_{XY}(r)$ decaying slowest [51]; we thus identify this to be the gapless XY QLRO phase.

Using these methods, the full topology of the phase diagram can be ascertained, depicted in Fig. 1(b); we more carefully determined the precise phase boundaries via the method of level spectroscopy; see the Supplemental Material [51] and Refs. [54,55] for details.

*DQC*—We hone in on the continuous QPT between the zAFM and VBS phases, which above investigations already strongly suggest is an example of DQC [24–26,65]. More insight is given by a field theory analysis: using the Jordan-Wigner transformation followed by bosonization [56], we obtain the continuum Hamiltonian [51]:

$$H \propto \int_0^L \mathrm{d}x \left[\frac{1}{K}(\partial_x\phi)^2 + K(\partial_x\theta)^2\right] + g_4 \cos 4\phi + \cdots. \quad (3)$$

Above, $K$ is the so-called Luttinger parameter; $\phi, \theta$ are bosonic fields obeying $[\phi(x), \partial\theta(x')] = i\pi\delta(x - x')$, so that original (spin) order parameters are expressed as

$$O_{\text{zAFM}} \sim \cos 2\phi, \qquad O_{\text{VBS}} \sim \sin 2\phi,$$
$$O_{\text{xAFM}} \sim \cos\theta, \qquad O_{\text{yAFM}} \sim \sin\theta. \quad (4)$$

The microscopic $\mathrm{U}(1)_z$ spin-rotation symmetry manifests as the transformation $\theta \mapsto \theta + \varphi$ for arbitrary $\varphi$, translation symmetry as $\phi \mapsto \phi + \pi/2$ and $\theta \mapsto \theta + \pi$, and site-centered inversion as $\phi \mapsto -\phi$. Therefore, symmetry-allowed terms beyond the parenthesis in Eq. (3) have the structure $\cos 4n\phi$. Now, for $K > 1/2$, it can be shown that all such terms are irrelevant under renormalization group flow so that the system is gapless (specifically, a Luttinger liquid), corresponding to the XY QLRO phase [66]. However, for $1/8 < K < 1/2$, the $n = 1$ term is relevant, so that nonzero $g_4$ leads to condensation of $\phi = 0$ or $\pi/4$ depending on sign, corresponding to the (gapped) zAFM and VBS phases. Crucially, at the critical point $g_4 = 0$, an enlarged U(1) symmetry, associated with $\phi \mapsto \phi + \beta$ for arbitrary $\beta$, is seen to emerge (recall higher order terms can be ignored [51]). This emergent symmetry, characteristic of a DQCP, implies that the ground state is invariant under a continuous transformation that rotates $O_{\text{zAFM}}$ into $O_{\text{VBS}}$ and back. Consequently, $C_{\text{zAFM}}(r)$ and $C_{\text{VBS}}(r)$ are expected to exhibit power-law decays with identical exponents, as verified in Fig. 2(d).

The boundary between the zAFM and VBS phases is in fact a line of DQCPs [yellow line of Fig. 1(b)]. To examine the critical properties along the line, we employed the level spectroscopy technique [51,54] to extract the Luttinger parameter varying from 0.5 at the bicritical point [white cross of Fig. 1(b)] to $\approx 0.137$ at the smallest value of $J_3/J_6$ we could reliably simulate [see Fig. 2(e)]. We expect that $K$ still decreases for even smaller $J_3/J_6$ down to $1/8$, whereupon the DQC becomes destabilized as the next-order term in Eq. (3) becomes relevant, which is expected to drive a discontinuous transition or phase coexistence [51]. Interestingly, interactions further than NNN appear crucial

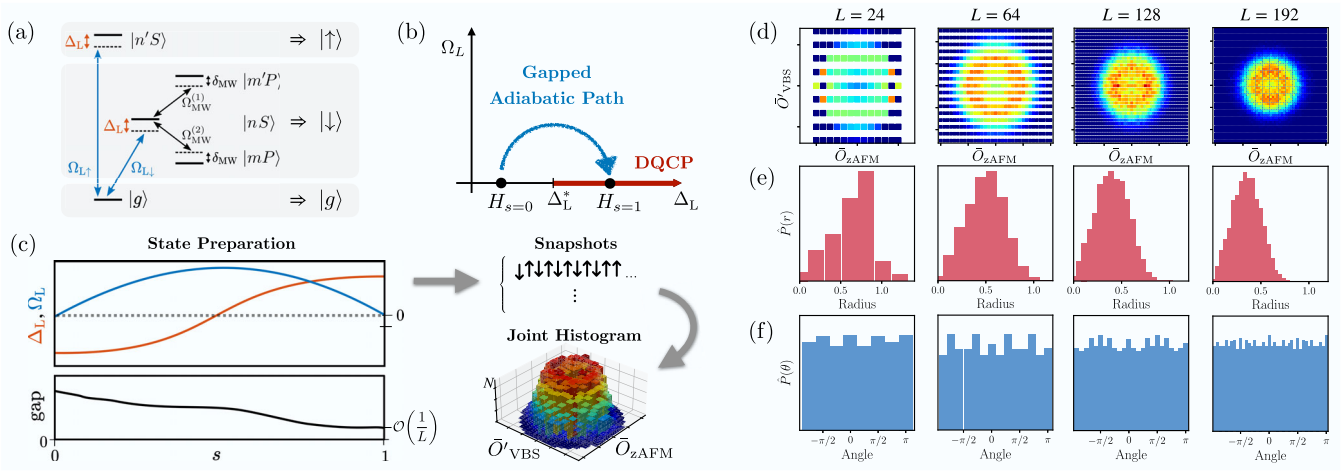


FIG. 3. (a) Proposed spin-state encoding enabling tunable $J_3/J_6$ couplings. We admix $|mP\rangle$ and $|m'P\rangle$ into $|nS\rangle$ via microwave drives of strengths $\Omega_{\mathrm{MW}}^{(1,2)}$ to form $|\downarrow\rangle$. Lasers with Rabi frequencies $\Omega_{\mathrm{L}\uparrow}/\Omega_{\mathrm{L}\downarrow}$ couple the ground state $|g\rangle$ to respective Rydberg spin states with detuning $\Delta_{\mathrm{L}}$, used in the state preparation protocol. (b) Schematic phase diagram of $H(s) \equiv H_{\mathrm{eff}} + H_{\ell}(s)$ and adiabatic path taken. (c) Ramp profiles of $\Omega_{\mathrm{L}}(s), \Delta_{\mathrm{L}}(s)$ considered for the state preparation, and accompanying many-body gap. (d)–(f) JPDs of order parameters $\bar{O}_{\mathrm{zAFM}}, \bar{O}'_{\mathrm{VBS}}$, and corresponding radial and angular distributions derived from $2 \times 10^4$ simulated measurement outcomes at the DQCP $(\alpha, J_3/J_6) \simeq (0.5, 0.597)$ for various system sizes.

to the small values of $K$ observed (see the Supplemental Material Fig. S2(e) and [51]).

*Experimental protocol.*—In order to realize the above physics in the laboratory, we have to address three challenges: (i) engineering $H_{\mathrm{eff}}$ with tunable parameters, (ii) devising an efficient protocol to prepare a critical ground state, and (iii) providing a measurement and data processing procedure to identify signatures of DQC.

Tunable $\alpha$ is easily achieved by geometrically rearranging atoms using optical tweezers. For tunable $J_3/J_6$, we propose encoding each spin state as an *admixture* of Rydberg states with different parities. As a concrete example, we choose $|\uparrow\rangle$ and $|\downarrow\rangle$ both as states of the same parity, denoted as $S$, and we further address $|\downarrow\rangle$ with two nearby states of opposite parity, denoted as $P$, using independent off resonant microwave drives [Fig. 3(a)]. Without admixing, VdW interactions between $S$ states give rise to $1/r^6$-decaying Ising-like couplings as already demonstrated in multiple experiments [31,33,34,57]. Admixing $P$ states generally introduces $1/r^3$-decaying dipolar interactions that contain both spin exchange and Ising couplings. Here, by judiciously choosing two different $P$ states, it is possible to engineer a negligible diagonal dipole moment of the dressed state, while keeping a substantial off diagonal (transition) dipole moment such that only exchange couplings are realized [58]. In this way, one can tune $J_3/J_6$ over a wide range, from nearly zero to greater than unity, with even a modest amount of admixture [51]. This realizes $H_{\mathrm{eff}}$ up to a uniform global Zeeman field, i.e., $\propto \sum_j Z_j$, which is inconsequential as long as our state preparation protocol lands us in the desired magnetization sector. We note that utilizing other microwave dressing schemes is possible [51] and also that exact engineering of $H_{\mathrm{eff}}$ is not needed as the existence of DQC is robust against perturbations.

To prepare the DQCP ground state, we propose an adiabatic protocol. Three remarks are in order: First, in experiments, atoms are typically initialized in their respective electronic ground states $|g\rangle^{\otimes L}$; thus, a state preparation protocol necessarily involves an extended Hilbert space of three internal states $\{|g\rangle, |\uparrow\rangle, |\downarrow\rangle\}$ per atom. Second, we desire to prepare the ground state of $H_{\mathrm{eff}}$ in the zero magnetization sector, which may not be the global ground state considered over all magnetization sectors. Finally, given finite coherence times in experiments, the many-body gap should ideally remain large throughout the adiabatic passage so that state preparation can be completed as quickly as possible while minimizing diabatic losses.

We present a many-body trajectory that satisfies all three criteria: $H(s) = H_{\mathrm{eff}} + H_{\ell}(s)$ with $s \in [0, 1]$, where $H_{\mathrm{eff}}$ is assumed to be tuned to a desired DQCP, and

$$H_{\ell}(s) = \sum_i \Omega_{\mathrm{L}}(s)(|\sigma(i)\rangle_i\langle g| + \mathrm{H.c.}) + \Delta_{\mathrm{L}}(s)\sum_i |g\rangle_i\langle g|$$

represents lasers coupling $|g\rangle$ to spin states $|\sigma(i)\rangle$ with $\sigma(i) = \uparrow(\downarrow)$ for even (odd) sites $i$, characterized by time-dependent Rabi frequencies $\Omega_{\mathrm{L}}(s)$ and detunings $\Delta_L(s)$ [Figs. 3(a)–3(c)]. Now, under a sufficiently slow, smooth ramp up of $\Delta_{\mathrm{L}}$ from a large negative to positive value while $\Omega_{\mathrm{L}}$ is switched on and off, all population from $|g\rangle$ will be transferred to the spin states [59]. Furthermore, $H(s)$ harbors two independent conserved quantities $N_A \equiv \sum_i (n^{\uparrow}_{2i} + n^{g}_{2i})$ and $N_B \equiv \sum_i (n^{\downarrow}_{2i-1} + n^{g}_{2i-1})$ throughout

the entire evolution since $[H(s), N_{A,B}] = 0$. Here, $n_i^a$ represents the occupation number operator for state $a$ at site $i$. This ensures that the final state has zero magnetization, provided all population in $|g\rangle$ is transferred, i.e., $n_i^g = 0$ for all $i$. Such a protocol thus ensures that the instantaneous ground state of $H(s = 0)$ is $|g\rangle^{\otimes L}$ while that of $H(s = 1)$ is the target DQCP. Finally, the choice of staggered couplings explicitly breaks translation symmetry except at the start and end of the trajectory, opening the many-body gap away from the DQCP, which we numerically observe [Figs. 3(b) and 3(c)].

To demonstrate the protocol's feasibility, we consider $\Omega_L(s) = J_6 \sin(\pi s)$ and $\Delta_L(s) = -2J_6 \cos(\pi s)$, fixing $(\alpha, J_3/J_6) = (0.5, 0.597)$ (i.e., a DQCP). Up to $L = 12$, we can perform exact simulations with realistic values $J_6 \sim 2\pi \times 25$ MHz (used in Ref. [57]) assuming a linear ramp $s(t) = t/T$, which reveals that a state with many-body overlap ~0.99 with the exact ground state can be prepared with the state-preparation time $T = 60/J_6 \sim 0.4$ μs, well within typical Rydberg lifetimes ~150 μs [57]. Furthermore, based on the Kibble-Zurek scaling ansatz [33,67,68], we find that the condition for the adiabaticity is $T \gtrsim L^{3-4K}$. Combined with exact numerical results, we estimate that a system of $L = 24$ can be prepared with a state-preparation time $T \sim 1$ μs, and $L = 64$ with $T \sim 5$ μs.

The smoking-gun signature of DQC is the emergent symmetry unifying different order parameters. We now argue this can be directly observed in Rydberg simulators. Naïvely, an explicit way to verify the emergent symmetry is to measure arbitrary linear combinations of order parameters $O_\eta = O_{\mathrm{zAFM}} \cos\eta + O_{\mathrm{VBS}} \sin\eta$ and to show that the distribution of $O_\eta$ behaves identically for any $\eta$ upon potential rescaling of $O_{\mathrm{zAFM}}$ and $O_{\mathrm{VBS}}$. This approach, however, is infeasible with existing experimental technologies as measuring $O_{\eta\neq 0}$ requires applying highly complicated unitary rotations before performing measurements in the standard $z$ basis. Instead, we can consider $O'_{\mathrm{VBS}}(r) \equiv (-1)^r (Z_{r+1}Z_r - Z_rZ_{r-1})$, which behaves identically to $O_{\mathrm{VBS}}(r)$ under symmetry transformations relevant to $H_{\mathrm{eff}}$, and hence serves as an alternative, but bona fide VBS order parameter [69]. Now $\bar{O}_{\mathrm{zAFM}}$ and $\bar{O}'_{\mathrm{VBS}}$ (bar denotes spatial averaging) are *simultaneously* evaluable within global measurement snapshots in the standard $z$ basis [Fig. 3(c)]. Such measurements in fact give access to the entire statistical properties of $\bar{O}_{\mathrm{zAFM}}$ and $\bar{O}'_{\mathrm{VBS}}$, captured by their joint probability distribution (JPD). Figures 3(d)–3(f) illustrate the JPD and corresponding radial-angular distributions, derived from simulated snapshots at a DQCP for various system sizes [51]. Already at $L = 24$, the rotational invariance between the order parameters can be gleaned, which becomes increasingly prominent with larger sizes. Note that this ring distribution would not arise if the transition were instead characterized only by a simple coexistence of zAFM and VBS orders: the JPD would have four distinct peaks, amounting to overlaying distributions of Figs. 1(c) and 1(e).

*Conclusion and outlook.*—In this Letter, we have studied a realistic 1D model of interacting neutral atoms, and showed that it hosts interesting quantum phases and transitions, including deconfined quantum criticality. We also proposed an experimental protocol to image the emergent symmetry associated with DQC, paving the way for a novel, categorical verification of this long sought-after, unconventional quantum criticality in Rydberg quantum simulators. Interestingly, we found that the Luttinger parameter $K$ characterizing the DQC behavior can be tuned in a wide range of values due to the presence of long-range interactions as illustrated in Fig. 2(e). Therefore, our proposal would also provide an opportunity to experimentally investigate the physics of coupled Luttinger liquids [71–74] in a systematic fashion.

This work is supported by various fundings from National Science Foundation (CUA, PHY-1734011; KITP, PHY-1748958; Aspen Center for Physics, PHY-1607611; CAREER awards, DMR-1847861 and DMR-2237244; and QLCI-CI-2016244), Department of Energy (Quantum Systems Accelerator Center, 7571809; and 032054-0000), Army Research Office (W911NF1910517), Gordon and Betty Moore Foundation (8690), and Singapore NRF Fellowship (NRFF15-2023-0008). Computing resources were administered by the Center for Scientific Computing and funded by NSF (CNS-1725797).

*jongyeon@illinois.edu

[1] T. Senthil, L. Balents, S. Sachdev, A. Vishwanath, and M. P. A. Fisher, Quantum criticality beyond the Landau-Ginzburg-Wilson paradigm, Phys. Rev. B **70**, 144407 (2004).

[2] T. Senthil, A. Vishwanath, L. Balents, S. Sachdev, and M. P. A. Fisher, Deconfined quantum critical points, Science **303**, 1490 (2004).

[3] A. Nahum, P. Serna, J. T. Chalker, M. Ortuño, and A. M. Somoza, Emergent SO(5) Symmetry at the Néel to Valence-Bond-Solid Transition, Phys. Rev. Lett. **115**, 267203 (2015).

[4] M. A. Metlitski and R. Thorngren, Intrinsic and emergent anomalies at deconfined critical points, Phys. Rev. B **98**, 085140 (2018).

[5] C. Wang, A. Nahum, M. A. Metlitski, C. Xu, and T. Senthil, Deconfined Quantum Critical Points: Symmetries and Dualities, Phys. Rev. X **7**, 031051 (2017).

[6] N. Ma, G.-Y. Sun, Y.-Z. You, C. Xu, A. Vishwanath, A. W. Sandvik, and Z. Y. Meng, Dynamical signature of fractionalization at a deconfined quantum critical point, Phys. Rev. B **98**, 174421 (2018).

[7] N. Ma, Y.-Z. You, and Z. Y. Meng, Role of Noether's Theorem at the Deconfined Quantum Critical Point, Phys. Rev. Lett. **122**, 175701 (2019).

[8] A. B. Kuklov, M. Matsumoto, N. V. Prokof'ev, B. V. Svistunov, and M. Troyer, Deconfined Criticality: Generic

First-Order Transition in the SU(2) Symmetry Case, Phys. Rev. Lett. **101**, 050405 (2008).
[9] G. Chen, J. Gukelberger, S. Trebst, F. Alet, and L. Balents, Coulomb gas transitions in three-dimensional classical dimer models, Phys. Rev. B **80**, 045112 (2009).
[10] J. Lou, A. W. Sandvik, and N. Kawashima, Antiferromagnetic to valence-bond-solid transitions in two-dimensional SU($n$) Heisenberg models with multispin interactions, Phys. Rev. B **80**, 180414(R) (2009).
[11] D. Charrier and F. Alet, Phase diagram of an extended classical dimer model, Phys. Rev. B **82**, 014429 (2010).
[12] A. Nahum, J. T. Chalker, P. Serna, M. Ortuño, and A. M. Somoza, 3D Loop Models and the cp$^{n-1}$ Sigma Model, Phys. Rev. Lett. **107**, 110601 (2011).
[13] K. Harada, T. Suzuki, T. Okubo, H. Matsuo, J. Lou, H. Watanabe, S. Todo, and N. Kawashima, Possibility of deconfined criticality in SU($n$) Heisenberg models at small $n$, Phys. Rev. B **88**, 220408(R) (2013).
[14] M. S. Block, R. G. Melko, and R. K. Kaul, Fate of $\mathbb{C}\mathbb{P}^{N-1}$ Fixed Points with $q$ Monopoles, Phys. Rev. Lett. **111**, 137202 (2013).
[15] L. Bartosch, Corrections to scaling in the critical theory of deconfined criticality, Phys. Rev. B **88**, 195140 (2013).
[16] Y. Q. Qin, Y.-Y. He, Y.-Z. You, Z.-Y. Lu, A. Sen, A. W. Sandvik, C. Xu, and Z. Y. Meng, Duality between the Deconfined Quantum-Critical Point and the Bosonic Topological Transition, Phys. Rev. X **7**, 031052 (2017).
[17] T. Sato, M. Hohenadler, and F. F. Assaad, Dirac Fermions with Competing Orders: Non-Landau Transition with Emergent Symmetry, Phys. Rev. Lett. **119**, 197203 (2017).
[18] H. Shao, Y. Q. Qin, S. Capponi, S. Chesi, Z. Y. Meng, and A. W. Sandvik, Nearly Deconfined Spinon Excitations in the Square-Lattice Spin-1/2 Heisenberg Antiferromagnet, Phys. Rev. X **7**, 041072 (2017).
[19] M. Ippoliti, R. S. K. Mong, F. F. Assaad, and M. P. Zaletel, Half-filled landau levels: A continuum and sign-free regularization for three-dimensional quantum critical points, Phys. Rev. B **98**, 235108 (2018).
[20] J. Y. Lee, C. Wang, M. P. Zaletel, A. Vishwanath, and Y.-C. He, Emergent Multi-Flavor QED$_3$ at the Plateau Transition between Fractional Chern Insulators: Applications to Graphene Heterostructures, Phys. Rev. X **8**, 031015 (2018).
[21] B. Zhao, P. Weinberg, and A. W. Sandvik, Symmetry-enhanced discontinuous phase transition in a two-dimensional quantum magnet, Nat. Phys. **15**, 678 (2019).
[22] P. Serna and A. Nahum, Emergence and spontaneous breaking of approximate O(4) symmetry at a weakly first-order deconfined phase transition, Phys. Rev. B **99**, 195110 (2019).
[23] J. Y. Lee, Y.-Z. You, S. Sachdev, and A. Vishwanath, Signatures of a Deconfined Phase Transition on the Shastry-Sutherland Lattice: Applications to Quantum Critical $SrCu_2(BO_3)_2$, Phys. Rev. X **9**, 041037 (2019).
[24] R.-Z. Huang, D.-C. Lu, Y.-Z. You, Z. Y. Meng, and T. Xiang, Emergent symmetry and conserved current at a one-dimensional incarnation of deconfined quantum critical point, Phys. Rev. B **100**, 125137 (2019).
[25] S. Jiang and O. Motrunich, Ising ferromagnet to valence bond solid transition in a one-dimensional spin chain: Analogies to deconfined quantum critical points, Phys. Rev. B **99**, 075103 (2019).
[26] C. Mudry, A. Furusaki, T. Morimoto, and T. Hikihara, Quantum phase transitions beyond Landau-Ginzburg theory in one-dimensional space revisited, Phys. Rev. B **99**, 205153 (2019).
[27] R.-Z. Huang and S. Yin, Kibble-Zurek mechanism for a one-dimensional incarnation of a deconfined quantum critical point, Phys. Rev. Res. **2**, 023175 (2020).
[28] B. Roberts, S. Jiang, and O. I. Motrunich, One-dimensional model for deconfined criticality with $\mathbb{z}_3 \times \mathbb{z}_3$ symmetry, Phys. Rev. B **103**, 155143 (2021).
[29] L. Zou and Y.-C. He, Field-induced QCD$_3$-Chern-Simons quantum criticalities in Kitaev materials, Phys. Rev. Res. **2**, 013072 (2020).
[30] K. Slagle, Y. Liu, D. Aasen, H. Pichler, R. S. K. Mong, X. Chen, M. Endres, and J. Alicea, Quantum spin liquids bootstrapped from Ising criticality in Rydberg arrays, Phys. Rev. B **106**, 115122 (2022).
[31] H. Bernien, S. Schwartz, A. Keesling, H. Levine, A. Omran, H. Pichler, S. Choi, A. S. Zibrov, M. Endres, M. Greiner, V. Vuletić, and M. D. Lukin, Probing many-body dynamics on a 51-atom quantum simulator, Nature (London) **551**, 579 (2017).
[32] S. de Léséleuc, V. Lienhard, P. Scholl, D. Barredo, S. Weber, N. Lang, H. P. Büchler, T. Lahaye, and A. Browaeys, Observation of a symmetry-protected topological phase of interacting bosons with Rydberg atoms, Science **365**, 775 (2019).
[33] A. Keesling, A. Omran, H. Levine, H. Bernien, H. Pichler, S. Choi, R. Samajdar, S. Schwartz, P. Silvi, S. Sachdev, P. Zoller, M. Endres, M. Greiner, V. Vuletić, and M. D. Lukin, Quantum Kibble–Zurek mechanism and critical dynamics on a programmable Rydberg simulator, Nature (London) **568**, 207 (2019).
[34] G. Semeghini, H. Levine, A. Keesling, S. Ebadi, T. T. Wang, D. Bluvstein, R. Verresen, H. Pichler, M. Kalinowski, R. Samajdar, A. Omran, S. Sachdev, A. Vishwanath, M. Greiner, V. Vuletić, and M. D. Lukin, Probing topological spin liquids on a programmable quantum simulator, Science **374**, 1242 (2021).
[35] T. M. Graham *et al.*, Multi-qubit entanglement and algorithms on a neutral-atom quantum computer, Nature (London) **604**, 457 (2022).
[36] M. C. Bañuls *et al.*, Simulating lattice gauge theories within quantum technologies, Eur. Phys. J. D **74**, 165 (2020).
[37] E. Lieb, T. Schultz, and D. Mattis, Two soluble models of an antiferromagnetic chain, Ann. Phys. (N.Y.) **16**, 407 (1961).
[38] E. Lieb, T. Schultz, and D. Mattis, *Condensed Matter Physics and Exactly Soluble Models* (Springer, New York, 2004).
[39] M. B. Hastings, Sufficient conditions for topological order in insulators, Europhys. Lett. **70**, 824 (2005).
[40] M. Oshikawa, Commensurability, Excitation Gap, and Topology in Quantum Many-Particle Systems on a Periodic Lattice, Phys. Rev. Lett. **84**, 1535 (2000).
[41] J. R. Parreira, O. Bolina, and J. F. Perez, Néel order in the ground state of Heisenberg antiferromagnetic chains with long-range interactions, J. Phys. A **30**, 1095 (1997).

[42] N. Laflorencie, I. Affleck, and M. Berciu, Critical phenomena and quantum phase transition in long range Heisenberg antiferromagnetic chains, J. Stat. Mech. (2005) P12001.

[43] M. F. Maghrebi, Z.-X. Gong, and A. V. Gorshkov, Continuous Symmetry Breaking in 1D Long-Range Interacting Quantum Systems, Phys. Rev. Lett. **119**, 023001 (2017).

[44] A. Zarubin, F. Kassan-Ogly, and A. Proshkin, Frustrations in the Ising chain with the third-neighbor interactions, J. Magn. Magn. Mater. **514**, 167144 (2020).

[45] C. K. Majumdar and D. K. Ghosh, On next-nearest-neighbor interaction in linear chain. I, J. Math. Phys. (N.Y.) **10**, 1388 (1969).

[46] S. R. White, Density Matrix Formulation for Quantum Renormalization Groups, Phys. Rev. Lett. **69**, 2863 (1992).

[47] S. R. White, Density-matrix algorithms for quantum renormalization groups, Phys. Rev. B **48**, 10345 (1993).

[48] U. Schollwöck, The density-matrix renormalization group, Rev. Mod. Phys. **77**, 259 (2005).

[49] In the DMRG simulation for infinite systems, the variationally optimized matrix product state explicitly breaks the symmetry in a spontaneously symmetry broken phase. Therefore, the order parameter expectation values for the resulting ground state can take finite values.

[50] P. Calabrese and J. Cardy, Entanglement entropy and conformal field theory, J. Phys. A **42**, 504005 (2009).

[51] See Supplemental Material at http://link.aps.org/supplemental/10.1103/PhysRevLett.131.083601, which includes Refs. [41–43,52–64] for detailed derivations and numerical simulation results that support the manuscript.

[52] V. L. Berezinskiĭ, Destruction of long-range order in one-dimensional and two-dimensional systems having a continuous symmetry group I. Classical systems, Sov. Phys. JETP **32**, 493 (1971).

[53] J. M. Kosterlitz and D. J. Thouless, Ordering, metastability and phase transitions in two-dimensional systems, J. Phys. C **6**, 1181 (1973).

[54] K. Nomura and K. Okamoto, Critical properties of s $= 1/2$ antiferromagnetic XXZ chain with next-nearest-neighbour interactions, J. Phys. A **27**, 5773 (1994).

[55] A. Ueda and M. Oshikawa, Resolving the Berezinskii-Kosterlitz-Thouless transition in the two-dimensional XY model with tensor-network-based level spectroscopy, Phys. Rev. B **104**, 165132 (2021).

[56] T. Giamarchi, *Quantum Physics in One Dimension*, International Series of Monographs on Physics (Clarendon Press, Oxford, 2004).

[57] A. Omran, H. Levine, A. Keesling, G. Semeghini, T. T. Wang, S. Ebadi, H. Bernien, A. S. Zibrov, H. Pichler, S. Choi, J. Cui, M. Rossignolo, P. Rembold, S. Montangero, T. Calarco, M. Endres, M. Greiner, V. Vuletić, and M. D. Lukin, Generation and manipulation of Schrodinger cat states in Rydberg atom arrays, Science **365**, 570 (2019).

[58] J. T. Young, P. Bienias, R. Belyansky, A. M. Kaufman, and A. V. Gorshkov, Asymmetric Blockade and Multiqubit Gates via Dipole-Dipole Interactions, Phys. Rev. Lett. **127**, 120501 (2021).

[59] I. I. Beterov, D. B. Tretyakov, V. M. Entin, E. A. Yakshina, I. I. Ryabtsev, M. Saffman, and S. Bergamini, Application of adiabatic passage in Rydberg atomic ensembles for quantum information processing, J. Phys. B **53**, 182001 (2020).

[60] A. Browaeys, D. Barredo, and T. Lahaye, Experimental investigations of dipole–dipole interactions between a few Rydberg atoms, J. Phys. B **49**, 152001 (2016).

[61] S. Weber, C. Tresp, H. Menke, A. Urvoy, O. Firstenberg, H. P. Büchler, and S. Hofferberth, Calculation of Rydberg interaction potentials, J. Phys. B **50**, 133001 (2017).

[62] S. Whitlock, A. W. Glaetzle, and P. Hannaford, Simulating quantum spin models using Rydberg-excited atomic ensembles in magnetic microtrap arrays, J. Phys. B **50**, 074001 (2017).

[63] M. P. Zaletel, R. S. K. Mong, C. Karrasch, J. E. Moore, and F. Pollmann, Time-evolving a matrix product state with long-ranged interactions, Phys. Rev. B **91**, 165112 (2015).

[64] P. Di Francesco, P. Mathieu, and D. Senechal, *Conformal Field Theory*, Graduate Texts in Contemporary Physics (Springer-Verlag, New York, 1997).

[65] F. D. M. Haldane, Spontaneous dimerization in the $s = \frac{1}{2}$ Heisenberg antiferromagnetic chain with competing interactions, Phys. Rev. B **25**, 4925 (1982).

[66] We ignored long-range terms $1/r^m$ with $m \geq 3$; if one writes down such a long-range interaction in terms of operators with positive scaling dimensions, the interaction can be shown to be always irrelevant.

[67] T. W. B. Kibble, Topology of cosmic domains and strings, J. Phys. A **9**, 1387 (1976).

[68] W. H. Zurek, Cosmological experiments in superfluid helium?, Nature (London) **317**, 505 (1985).

[69] From the field-theoretic derivation [70], $O'_{\mathrm{VBS}}$ can be shown to behave as $\sin 2\phi$ as well. Also, due to the emergent singlet nature of the VBS phase, correlations in $X$, $Y$, $Z$ are approximately similar which we verified numerically throughout the phase.

[70] E. Orignac and T. Giamarchi, Weakly disordered spin ladders, Phys. Rev. B **57**, 5812 (1998).

[71] R. Mukhopadhyay, C. L. Kane, and T. C. Lubensky, Crossed sliding Luttinger liquid phase, Phys. Rev. B **63**, 081103(R) (2001).

[72] R. Mukhopadhyay, C. L. Kane, and T. C. Lubensky, Sliding Luttinger liquid phases, Phys. Rev. B **64**, 045120 (2001).

[73] E. Plamadeala, M. Mulligan, and C. Nayak, Perfect metal phases of one-dimensional and anisotropic higher-dimensional systems, Phys. Rev. B **90**, 241101(R) (2014).

[74] E. Leviatan and D. F. Mross, Unification of parton and coupled-wire approaches to quantum magnetism in two dimensions, Phys. Rev. Res. **2**, 043437 (2020).